Patterned and Ordered Metal Nanoparticle Arrays – Templates for Functional Nanoscale Architectures

File No. SR/S3/CE/60/2005

A Project Completion Report

Submitted to SERC-DST

by

S. VENUGOPAL
ASSISTANT PROFESSOR
DEPARTMENT OF CHEMICAL ENGINEERING

INDIAN INSTITUTE OF SCIENCE
BANGALORE 560012, INDIA

February, 2010

1. *Title of the project:* Patterned and Ordered Metal Nanoparticle Arrays – Templates for Functional Nanoscale Architectures

2. *Principal Investigator(s) and Co-Investigator(s):* Santhanam Venugopal (PI), Sanjeev Kumar Gupta (Co-PI)

3. *Implementing Institution(s) and other collaborating Institution(s):* Indian Institute of Science

4. *Date of commencement:* 01-06-2006

5. *Planned date of completion:* 30-11-2009

6. *Actual date of completion:* 30-11-2009

7. *Objectives as stated in the project proposal:*

    - Development of a plasma processing route for the fabrication of uniform, patterned, and ordered arrays of bare gold nanoparticle mono/multilayers from Monolayer Protected Nanoparticle (MPN) arrays.
    - Optimization of plasma parameters using spectroscopic characterization of the rate of removal of alkanethiol monolayers from the surface of gold nanoparticles.
    - Thermal stability analysis of bare gold nanoparticle arrays on various substrates.

8. *Deviation made from original objectives if any, while implementing the project and reasons thereof:*
    - A green, room-temperature protocol for metal nanoparticle synthesis was developed as part of our effort to synthesize gold nanoparticles. As this protocol is a promising avenue for large-scale nanoparticle synthesis, detailed investigation of the batch protocol was also undertaken. Apart from this, some preliminary experiments on using gold nanoparticle arrays as templates for ordered nanowire array synthesis was also carried out (with the help of Prof. K.K. Nanda, MRC, IISc)

9. *Experimental work giving full details of experimental set up, methods adopted, data collected supported by necessary table, charts, diagrams & photographs. Detailed analysis of results indicating contributions made towards increasing the state of knowledge in the subject:*

9.1 Synthesis of gold nanoparticles:-

Tannic acid, a plant based polyphenol, was used to rapidly (on the order of minutes) synthesize size-controlled gold and silver nanoparticles under ambient conditions. We systematically investigated the effect of pH on the size distribution of nanoparticles synthesized. Based on induction time and ζ-potential measurements, we show that particle size distribution is controlled by a fine balance between the rates of reduction (determined by the initial pH of reactants) and coagulation (determined by the pH of the reaction mixture) in the initial period of growth. This insight led to the optimal batch process for size-controlled synthesis of 2-10 nm gold nanoparticles— slow addition of chloroauric acid into tannic acid.

9.1.2. Experimental methods

9.1.2.1 Materials

Hydrogen tetrachloroaurate (III) hydrate (99.999%) and tannic acid (ACS reagent) were purchased from Sigma-Aldrich Co. The replicate experiments reported in figure 7 were carried out using chemicals of similar purity purchased from Acros organics ltd. Potassium carbonate was purchased from Merck Co. Deionized water obtained from a MilliQ® system was used in all the experiments. All chemicals were used as received.

9.1.2.2 Synthesis of gold nanoparticles

The experiments were carried out in glassware cleaned with aquaregia (1:3 volumetric ratio of nitric acid to hydrochloric acid, CAUTION: Aquaregia solutions are extremely corrosive. They must be handled with appropriate protective equipment and with extreme care), rinsed thoroughly with deionized water and then dried in air prior to use. For the preliminary investigations and experiments 'A' – 'F', the precursor solutions were prepared as follows. 0.25 mL of 25.4 mM chloroauric acid solution was made up to 22 mL using DI water. 3 mL of the desired concentration of tannic acid solution was prepared. 150 mM potassium carbonate solution was used to adjust the pH of tannic acid and/or chloroauric acid solution. If necessary, 0.1 N hydrochloric acid was used to adjust the pH of chloroauric solution. A reactor equipped with home-made Rushton turbine and baffles of standardized design machined out of Teflon was used to mix the reactants (macroscopic blending time of 2s). Typically, chloroauric acid solution was taken in the stirred vessel and the reducing agent was added as one portion (within 1 second). The reaction mixture was stirred till the colour of the colloidal solution did not appear to change.
For stop flow module studies (experiment 'H'), stock solutions of chloroauric acid and tannic acid were prepared as follows. Briefly, 0.25 mL of 25.4 mM chloroauric acid was made up to 20 mL using DI water. 2.25 mL of 5.9 mM tannic acid was made up to 5 mL using DI water.
Experiment 'I' was carried out by adding 10 mL of 0.64 mM chloroauric acid solution (pH-3.2) slowly (dropwise,~ 1 mL/min) into 15 mL of 0.89 mM tannic acid solution (pH-7.1) that was being stirred. The total volumes and amounts of reagents used were kept at the same value as experiment 'B' and 'G'. For seeded growth experiment reported in figure 6f, 2.5 mL (from a total of 25 mL) of the solution formed in experiment 'I' was made upto 15 mL using DI water and 10 mL of 0.32 mM chloroauric acid solution was added slowly (dropwise) into it. The pH was adjusted to be above 6.4 by intermittently adding required quantities of 150 mM potassium carbonate solution.

9.1.2.3 Sample characterization

Transmission Electron Microscopy (TEM) characterization was performed using a Tecnai F30 operating at 200 KV. Samples for TEM were prepared by drop casting about 18 drops (~1 mL) of the sample on a carbon film coated copper grid that was placed on a lint-free tissue paper. ImageJ (http://rsbweb.nih.gov/ij) software was used for analysing TEM images after applying an appropriate threshold. At least 300 particles, at the same magnification from different images of various regions on the TEM grid, were counted to obtain the reported nanoparticle size distributions. The mean ($\mu \equiv \Sigma d_i / n$) and standard deviation ($\sigma \equiv \sqrt{(\Sigma(d_i - \mu)^2/(n-1))}$) of the nanoparticle size distribution are reported along with the size histograms displaying the actual number of particles counted.
UV-Vis spectroscopy was carried out in absorbance mode using a Systronics double beam UV visible spectrophotometer 2201. DI water was used as the reference. Stop flow reactor (SFM-400, Biologic SA, Claix, France) equipped with xenon lamp and photomultiplier tube was used to monitor (dead time~ 3 ms), with 10 μs time resolution, the absorbance of the reaction mixture at the desired wavelength after rapid mixing of the reactants. Chloroauric acid and tannic acid were mixed in

a volumetric ratio of 4:1 to mimic the ratio used in batch experiments. The induction time was determined as the time at which there was a detectable change in slope of the absorbance vs. time profiles.
The % yield (ratio of gold present in nanoparticles to that present in the precursor solution) of the synthesis was measured by carrying out Atomic Absorption Spectrometry of gold precipitate using GBC Avanta 3000 (graphite furnace). Standard curve method was used for calibration. Gold atomic absorption standard solution (Aldrich) was used to prepare standards of concentrations 0 ppb, 25 ppb, 50 ppb, 75 ppb and 100 ppb. The sampling volume was 20 μL. Average absorbance value (area under the peak) of four repetitions was calculated and a calibration curve was prepared. The 95% confidence limit for concentration values at a given absorbance was determined. Absorbance of the unknown solution was measured and the corresponding concentration was found using the calibration curve. For sample preparation, 5 mL of colloidal gold solution was precipitated by the addition of 5 mL of ethanol and 3 μL of dodecanethiol followed by centrifugation at 3000g for 30 min. The nanoparticle precipitate was then dissolved in 5 mL of aquaregia. Assuming complete conversion, a 100 ppb solution of the analyte sample was prepared by dilution. The minimum detection limit based on the calibration curve of AAS was 3.07 ppb.
The average hydrodynamic particle size (d_h) was measured at 90° scattering angle using a Dynamic Light Scattering (DLS) instrument (Model BI-200SM) from Brookhaven Co. equipped with BI-9000AT correlator system. The sample cells were cleaned with 2% Micron-90® solution (Cole-Parmer) at 60°C, followed by rinsing with deionized water and ethanol. The nanoparticle samples were not filtered prior to measurement. The concentration of the sample was decreased until the intensity detected decreases with dilution (to preclude multiple scattering effects) as per ISO 13321. Only results with a baseline difference of the intensity autocorrelation function that is less than 1 % were considered for analysis. The Non-Negatively constrained Least Squares (NNLS) algorithm was used for calculating the inverse Laplace transform of the autocorrelation data. The resultant intensity ($I \sim d^6$) weighted particle size distribution plot was used to report the average size of the dominant mode, which was selected based on the volume ($\sim d^3$) present in that mode. Typically, >90% of the resultant particles were present in the dominant mode selected and <5% of the particles had sizes >100 nm (presumed to be polymerized tannic acid or flocculates of nanoparticles). A Gaussian curve was fitted to the dominant mode using Origin® software to estimate the particle size (d_h). DLS measurements were repeated six times for each sample, the averaged results of these six repeated measurements are reported along with the standard deviation of these six estimates based on recommendations in the international standard, ISO 13321. It was observed that hydrodynamic size obtained from DLS was always greater than TEM mean diameter indicating the presence of an adsorbed layer, and the variability in measured hydrodynamic size was very sensitive to the presence of non-spherical particles.
ζ-potential values of gold colloidal solutions were measured either using a ZetaPlus analyzer from Brookhaven instruments or a Malvern Zetasizer, and the mean and standard deviation values based on three repeated measurements are reported. pH measurements were made using Orion™ pH electrode and benchtop meter.
The redox potential of freshly prepared 0.53 mM tannic acid solution (corresponding to MR 2.08) at different pH was measured using a saturated calomel electrode (SCE) as reference and platinum wire as the working electrode. The values reported are with respect to SCE, and were measured after allowing sufficient time to equilibrate.

9.1.3. Results and discussion

9.1.3.1 Variation of mean nanoparticle size with MR value

In preliminary experiments, we synthesized gold colloids at various MR values without altering the natural pH of the solutions. All the MR values chosen were greater than the stoichiometric requirement [based on our studies on the formation of silver nanoparticles] for complete reduction of gold salt. A few experiments carried out at different overall concentrations of gold chloride and tannic acid (varied from 25% to 200% of the standard value used) also yielded the same final nanoparticle size distribution as the samples reported herein for the corresponding MR values.
Figure 1a shows the variation of UV-Vis spectra as a function of the MR value. The surface plasmon resonance (SPR) peak in the UV-Vis spectra of gold nanoparticle solutions formed at MR values higher than 2.08 were red shifted with respect to those formed at lower MR values, indicating the presence of large particles, while those formed at MR values below 2.08 exhibit increased absorbance in the NIR region indicating the presence of anisotropic and faceted particles. Figure 1b shows the variation of hydrodynamic diameter with MR; the trend is in accord with that observed in UV-Vis spectra, with a minimum at MR value of 2.08. Representative TEM images of a few of these samples are also shown in figures 1c-1e, and the trend in the mean size is in agreement with UV-Vis and DLS data.

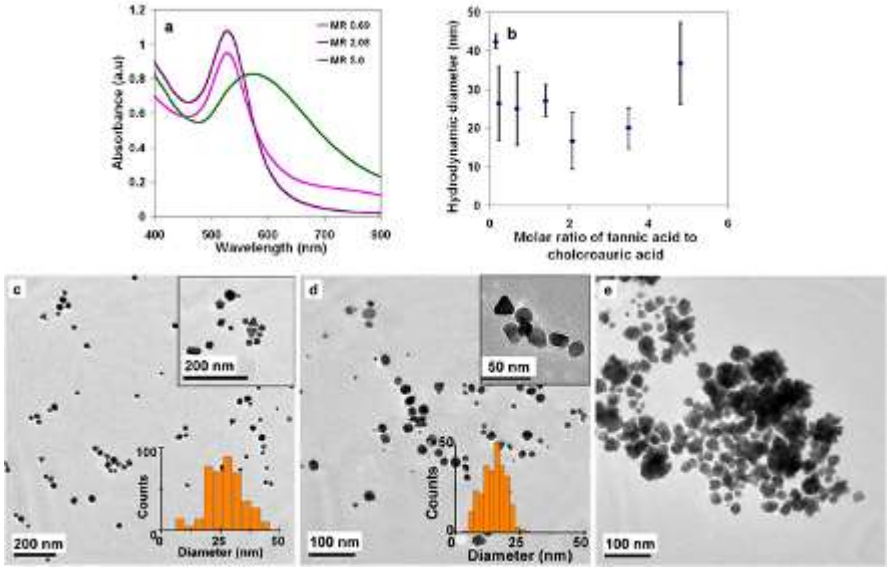

Figure 1. Effect of varying the molar ratio of tannic acid to chloroauric acid (MR). (a) UV visible spectra of colloids synthesized at different MR values. A red shift is observed in the surface plasmon peak beyond MR value of 2.08. (b) Variation of hydrodynamic diameter with MR. The error bars represent the standard deviation of the estimates of mean size obtained from six repeated measurements. (c) – (e) Representative TEM image of nanoparticles synthesized at different MR values. Insets show higher magnification images and size distribution histograms. (c), MR 0.69. Nanoparticle diameter ($\mu \pm \sigma$) = 25.3 ± 8.0 nm. (d) MR 2.08. Nanoparticle diameter ($\mu \pm \sigma$) = 14.1 ± 4.8 nm. (e) MR 5.2.

The TEM image of the sample prepared at MR values > 5.2 have several branched flower-like particles, which are ideal candidates for biomedical applications. The mean size (diameter of an equivalent circle having the same projected area) is not reported due to the highly irregular shape of the particles. The TEM image of the sample prepared at MR value of 0.69 shows that many particles are highly faceted with triangular or bipyramidal shapes, while the sample prepared at MR value of 2.08 shows predominantly quasispherical particles and a smaller fraction of particles with triangular/bipyramidal shapes. Furthermore, AAS analysis of the sample prepared with an MR 2.08 indicated that the yield was 90.8 ± 5.6 %(95% confidence limits), and that there was no gold remaining in the supernatant (within detectable limits, i.e. >3.07 %). This proves the quantitative conversion of gold present as ions in the precursor into atoms constituting the nanoparticles. The non-monotonic variation with MR of the size and shape of nanoparticles is currently under investigation as simple arguments based on increased reactivity and stabilisation due to an increase in tannic acid concentration cannot explain the minima. A detailed model that can explain these trends is being developed. As the objective is to synthesize spherical gold nanoparticles rapidly, further experiments were all carried out at an overall MR value of 2.08.

9.1.3.2 Role of pH

Ostwald cautioned that the pH of the chloroauric acid precursor solution had to be near neutral to ensure the stability (based on formation of a ruby coloured solution) of the resultant dispersion formed by reduction with tannin at its natural pH, which is acidic. Typically, changes in gold nanoparticle size or shape distributions resulting from a change in pH of the reaction mixture are ascribed to either a variation in the reactivity of the precursors and/or the strength of stabilization of nanoparticles. As the pH values required for maximising precursor reactivity and nanoparticle stabilisation differ significantly, we decided to explore conditions under which both reactivity and stabilisation could be optimised. So, we carried out a series of experiments under ambient conditions, by varying the initial pH of the two precursor solutions and characterized the resulting colloidal samples using TEM, induction time, and ζ-potential measurements. In the following, we focus our discussion on six experiments (labelled 'A' – 'F'), which provide an insight into the various processes modulated by changes in pH that affect the observed particle size distribution. The experimental conditions used, and the results of sample characterizations are presented in table 1. Representative TEM images of these samples are shown in figure 2. The measured lattice spacing (0.232 ± 0.008 nm) of the fringes seen in the inset of figure 2b corresponds to the value expected for gold (111).

Table 1. Summary of experimental conditions and characterization results.

Label	Initial pH of chloroauric acid solution	Initial pH of tannic acid solution	pH of reaction mixture	Particle diameter[a] ($\mu \pm \sigma$), nm	Induction time[b], s	ζ-potential[c], mV
A	3.2	3.1	3.2	14.1 ± 4.8	3	-20 ± 2
B	3.2	7.1	6.4	7.1 ± 1.6	1.5	-49 ± 2
C	7.0	6.3	6.4	10.7 ± 3.8	66.8	-69 ± 2
D	9.1	3.1	6.4	14.2 ± 5.4	163.5	-60 ± 2
E	2.1	7.1	5.0	10.0 ± 2.9	0.9	-18 ± 7
F	2.1	9.0	7.1	5.8 ± 1.0	0.5	-35 ± 7

a – based on TEM images. b – determined using a stop-flow module (SFM) as the time taken from mixing the reagents to the appearance of surface plasmon peak corresponding to gold nanoparticles. c – ζ-potential values were obtained using a Brookhaven Zetaplus ('A' – 'D') or a Malvern Zetasizer ('E' and 'F').

Experimental runs 'A' and 'B' were carried out to investigate the effect of varying the reactivity of tannic acid on nanoparticle synthesis. It is seen that both the nanoparticle mean diameter and polydispersity reduces upon an increase in tannic acid pH. Since the reduction in induction time (a measure of reactivity) is moderate while the ζ-potential changes significantly from -20 mV to -49 mV, the observed decrease in mean size and polydispersity is mainly attributed to a decrease in coalescence caused by increased strength of stabilization in experiment 'B'. Given that both these samples were stable upon storage for more than a year, coalescence is inferred to occur mainly during the initial period of nanoparticle growth. This supposition, i.e. that the value of ζ-potential measured in experiment A (-20 mV) is below the threshold for stabilizing small (< 2 nm) nanoparticles.

To study the effect of precursor reactivity on nanoparticle synthesis, experiments 'C' and 'D' were conducted by varying the pH of reagents while ensuring that the resultant reaction mixture pH was the same as in experiment 'B'. It is observed that the nanoparticle size and polydispersity increase with an increase in the initial pH of the chloroauric acid solution. The ζ-potential values measured in experiments 'B', 'C', and 'D' are sufficiently above the threshold value to preclude coalescence as the major factor responsible for the observed changes in nanoparticle size distribution amongst these three cases. The large increase in induction time clearly indicates that it is the decrease in chloroauric acid reactivity at higher pH values that results in small nucleation rates and prolonged nucleation periods (as nucleation will continue till sufficient nanoparticle surface area is generated for growth to dominate), thereby accounting for the observed changes in nanoparticle size distribution at the same overall reaction mixture pH. However, this deduction presumes that the reactivity of chloroauric acid is dependent on its initial pH and not on the reaction mixture pH.

It is reported that chloroauric acid is present mainly as a combination of gold chloro-hydroxy species in aqueous solutions, and that the reactivity decreases as the chloride ligands are displaced by hydroxyl ligands at higher pH values. It is also known that the absorbance at 315 nm corresponding to the charge transfer to solvent (CTTS) absorption band depends on the number of chloride ligands present. So, SFM experiments were conducted to study the effect of a sudden change in pH on the transformation of chloroauric acid species from one form into another, by monitoring the CTTS band of gold chloride at 315 nm. Figure 3a shows that the response time for chloroauric acid species transformation is of the order of 3-4 minutes, for a change in pH from 3.2 to 6.4. As this timescale is larger than the timescale for completion of reaction in experiment B, it indeed establishes that the reactivity of chloroauric acid solution is controlled by its initial pH and not the reaction mixture pH.

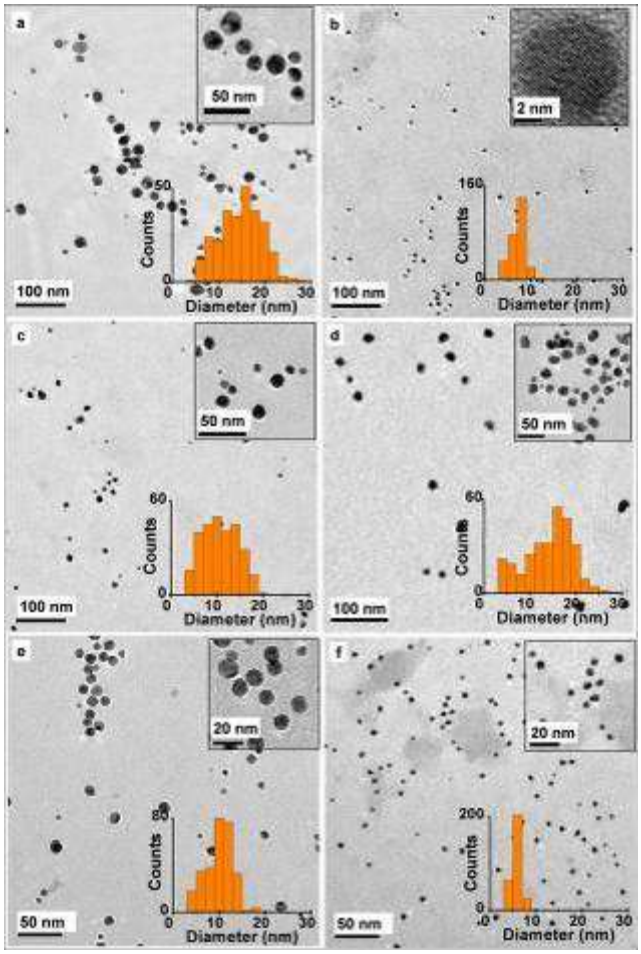

Figure 2. Representative TEM images of nanoparticles synthesized by varying reactant pH. Insets show higher magnification images and size distribution histograms. (a) Tannic acid at pH 3.1 was added to chloroauric acid at pH 3.2. Nanoparticle diameter ($\mu \pm \sigma$) = 14.1 ± 4.8 nm. (b) Tannic acid at pH 7.1 was added to chloroauric acid at pH 3.2. Nanoparticle diameter ($\mu \pm \sigma$) = 7.1 ± 1.6 nm. (c) Tannic acid at pH 6.3 was added to chloroauric acid at pH 7.0. Nanoparticle diameter ($\mu \pm \sigma$) = 10.7 ± 3.8 nm. (d) Tannic acid at pH 3.1 was added to chloroauric acid at pH 9.1. Nanoparticle diameter ($\mu \pm \sigma$) = 14.2 ± 5.4 nm. (e) Tannic acid at pH 7.1 was added to chloroauric acid at pH 2.1. Nanoparticle diameter ($\mu \pm \sigma$) = 10.0 ± 2.9 nm. (f) Tannic acid at pH 9.0 was added to chloroauric acid at pH 2.1. Nanoparticle diameter ($\mu \pm \sigma$) = 5.8 ± 1.0 nm.

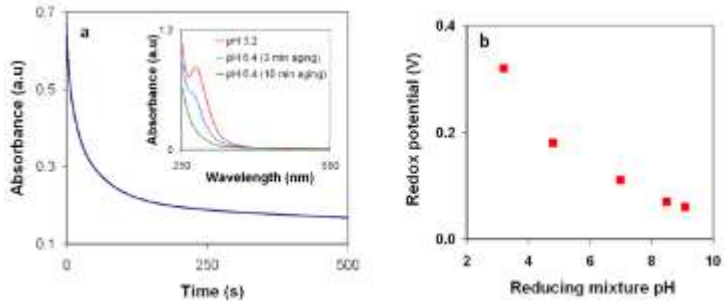

Figure 3. (a) The dynamics of absorbance at 315 nm monitored using an SFM at ms resolution, after rapidly mixing chloroauric acid solution at pH 3.2 with K_2CO_3 solution to change the pH to 6.4. The inset shows UV-Vis spectra (measured ex-situ) of a similar solution at various time intervals after increasing the pH from 3.2 to 6.4. (b) Redox potential (w.r.t. SCE) of tannic acid at different pH.

To delineate the effect of the reaction mixture pH from that of precursor reactivity, experiments 'E' and 'F' were conducted with chloroauric acid maintained at pH 2.1 and tannic acid at pH 7.1 and 9, this resulted in final reaction mixture pH values of 5.0 and 7.1 respectively. The redox potential of tannic acid increases only slightly over this range (fig. 3b), while chloroauric acid is expected to be in a more reactive state than in experiment 'B'. The measured values of induction time (0.9 and 0.5 s) are in agreement with these expectations. However, the observed value of nanoparticle size distribution (10.0 ± 2.9

nm) in experiment 'E' is larger than that in experiment 'B' (7.1 ± 1.6 nm), while that observed in experiment 'F' (5.8 ± 1.0 nm) is smaller. The ζ-potential values measured in experiments 'E' and 'F' (-18 and -35 mV) clearly indicate that the strength of stabilization has substantially decreased in the case of experiment 'E', signifying that coalescence was the reason for the observed larger size and polydispersity.

Comparing the data from experiments 'A', 'B', 'E' and 'F', it is clear that the strength of stabilization (as characterized by the magnitude of ζ-potential) is a function of reaction mixture pH and it changes considerably over a narrow range of pH (5.0 – 6.4) similar to the trend observed for the variation of redox potential with pH. Given that tannic acid is a weak acid with a pKa value of 5.12, these observations suggest that ionised tannin molecules aid in the reduction of chloroauric acid and they also act as the charge determining ions for stabilisation. The estimated trend in the degree of dissociation is found to correlate with reaction mixture pH and not with the initial pH of tannic acid solution. This is plausible as tannin molecules are charged by dissociation of phenolic H^+ ions, and this process responds rapidly to changes in environmental pH brought about by mixing.

Overall, these results show that gold nanoparticle size distribution is determined by a fine balance between the reactivity of precursors and coalescence in the initial period, which can be manipulated by controlling the initial pH of reactants and reaction mixture pH respectively. Figure 4 is a schematic illustration of the various pathways described earlier. An important outcome is that independent control over reactivity and stabilisation can be achieved by manipulating the pH of the precursor solutions.

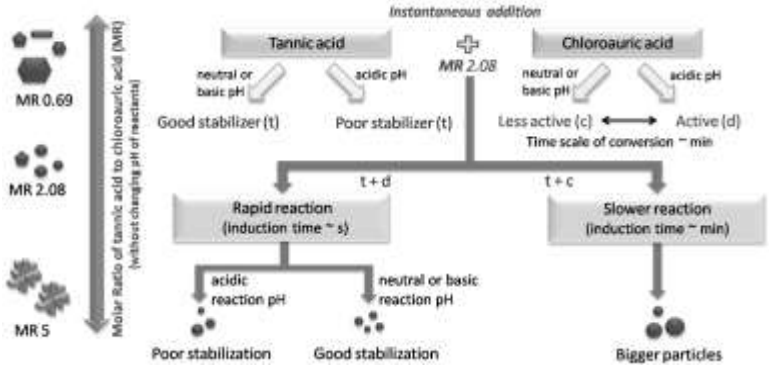

Figure 4. Schematic summary of the effect of MR and the roles of reagent and reaction mixture pH in determining nanoparticle size and shape.

9.1.3.3 Effect of varying addition protocols

As the objective is to achieve size-control, we focused our attention on experiment 'B', which exhibited the desirable characteristics of rapid nucleation and high stability (Note: experiment 'F' was not considered because of the need to add both an acid and a base for adjusting pH, which can lead to large variations in ionic strength and affect colloidal stability). In experiment 'B', tannic acid was added as one portion into chloroauric acid solution and so, during the initial period of mixing (mixing timescale ~ 2 s) an acidic environment was present around the growing nanoparticles possibly leading to coalescence.

Hence, an experiment ('G') was carried out to minimize coalescence during mixing by altering the order of addition such that the growing nanoparticles were typically in alkaline medium. This was achieved by simply reversing the order of addition (i.e. chloroauric acid into tannic acid), while maintaining the initial pH of reagents, overall amount of reagents, the volume of the added reagent, and the volume of the total reaction mixture at values used in experiment 'B'. For comparison, a 1 mL sample was prepared by rapidly mixing (~ in 3 ms) the two reagents in SFM (experiment H), while maintaining the concentration, initial pH and volumetric ratio similar to experiment 'B'.

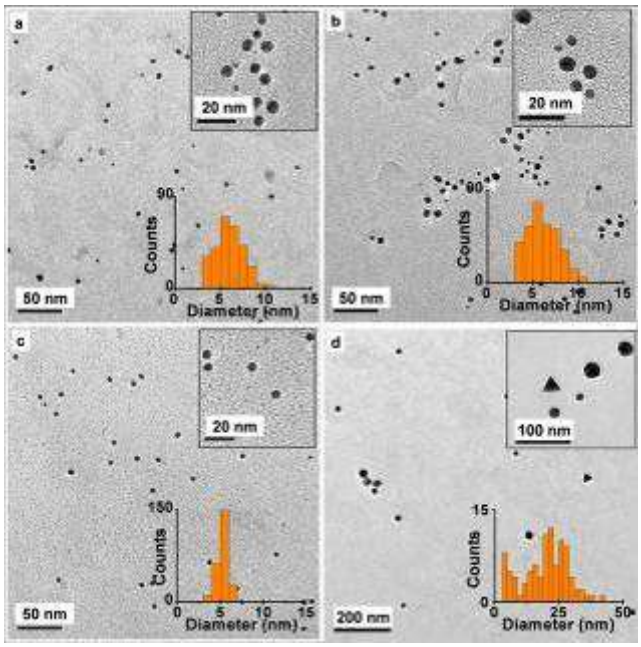

Figure 5. Representative TEM images highlighting the effect of order of addition, and rate of addition. Insets show higher magnification images and size distribution histograms. (a) Chloroauric acid added as one portion into tannic acid. Nanoparticle diameter ($\mu \pm \sigma$) = 5.9 ± 1.6 nm. (b) Chloroauric acid and tannic acid were rapidly mixed using SFM. Nanoparticle diameter ($\mu \pm \sigma$) = 6.2 ± 1.9 nm. (c) Chloroauric acid added slowly (1 mL/min) into tannic acid. Nanoparticle diameter ($\mu \pm \sigma$) = 5.3 ± 0.7 nm. (d) Tannic acid added slowly (1 mL/min) into chloroauric acid. Nanoparticle diameter ($\mu \pm \sigma$) = 15.8 ± 11.6 nm.

Figures 5a and 5b show representative TEM images of nanoparticles formed in experiments 'G' and 'H', and their corresponding size distributions are determined to be 5.9 ± 1.6 nm and 6.2 ± 1.9 nm respectively. The observed mean sizes follow the expected trend. The effect on standard deviation is however minimal, even in the case of rapid mixing, indicating that stabilization of nanoparticles by adsorption of tannin requires a finite time during which particles may coalesce. Attempts to ameliorate this situation by using an excess of tannic acid did not yield the desired result. So, the next best strategy was to add diluted chloroauric acid slowly into tannic acid to result in an optimal particle number density, which would suppress coalescence in the initial period and provide adequate time for adsorption of tannin. Experiment 'I' was conducted by adding chloroauric acid at a rate of ~1 mL/min into a pool of tannic acid, while maintaining overall concentration and total volume of reaction mixture constant as in experiment 'G' (see methods for further details). For comparison, experiment 'J' was conducted by adding tannic acid slowly into a pool of chloroauric acid, keeping volume added, overall amounts and total volume same as in experiment 'G' and 'I'.
Figures 5c and 5d show representative TEM images of nanoparticles formed in experiments 'I' and 'J'; their corresponding size distributions were determined to be 5.3 ± 0.7 nm and 15.8 ± 11.6 nm respectively. The narrow standard deviation observed in experiment 'I' confirms that it is the dynamics of tannin adsorption that controls coalescence in the initial period. Considering that the mean size is smaller than in experiment 'G' for the same amount of gold atoms used, it is clear that the nanoparticle number density obtained (~6.4 x10^{13} particles/mL) is higher than those obtained using the fast addition protocol. Carrying out slow (dropwise) addition of the same amount of chloroauric acid into tannic acid at different concentrations (i.e. different MR values) also resulted in quasi-spherical particles with lesser standard deviation as compared to the instantaneous addition protocol. In the case of experiment 'J', the rather large size and polydispersity are attributed to the presence of nanoparticles with different shapes and morphology. The observed faceted nature of nanoparticles is in agreement with that reported for nanoparticles growing in an environment of excess chloride at acidic pH.

9.1.3.4 Size-control by slow addition

Given that the slow (dropwise) addition method for a rapid precipitation reaction is akin to a seeded growth approach after an initial period, we conjectured that smaller sized nanoparticles would be formed by simply adding lesser amount of chloroauric acid to the mixture. Figures 6a-6d summarize the results of such a set of experiments wherein particles ranging from 1.7 nm to 3.8 nm have been synthesized at room temperature within a matter of minutes. The constant value of standard deviation estimates (0.6-0.8 nm), limited by errors associated with thresholding of TEM images for particle size analysis , indicates that the growth is surface reaction controlled (i.e. the growth rate is independent of particle size). This

process can be easily extended to form size-controlled nanoparticles with larger mean size, if care is taken to ensure that the reaction mixture pH never falls below 6.4. Figure 6e shows one such result obtained after the addition of 4x the amount of chloroauric acid used in experiment 'I'. The nanoparticle size distribution is found to be 7.4 ± 0.6 nm, which reaffirms the surface-reaction controlled nature of the growth mechanism. The processing time required to form size controlled nanoparticles in the range of 2-10 nm can be further reduced by maximizing the amount of chloroauric acid for a given volume and number density of seeds (too high a concentration leads to secondary nucleation). Figure 6f shows particles with a size distribution of 9.1 ± 0.7 nm that were formed within 10 minutes by optimizing the concentration of chloroauric acid for a seed density of 6.4 $x10^{12}$ particles/mL.

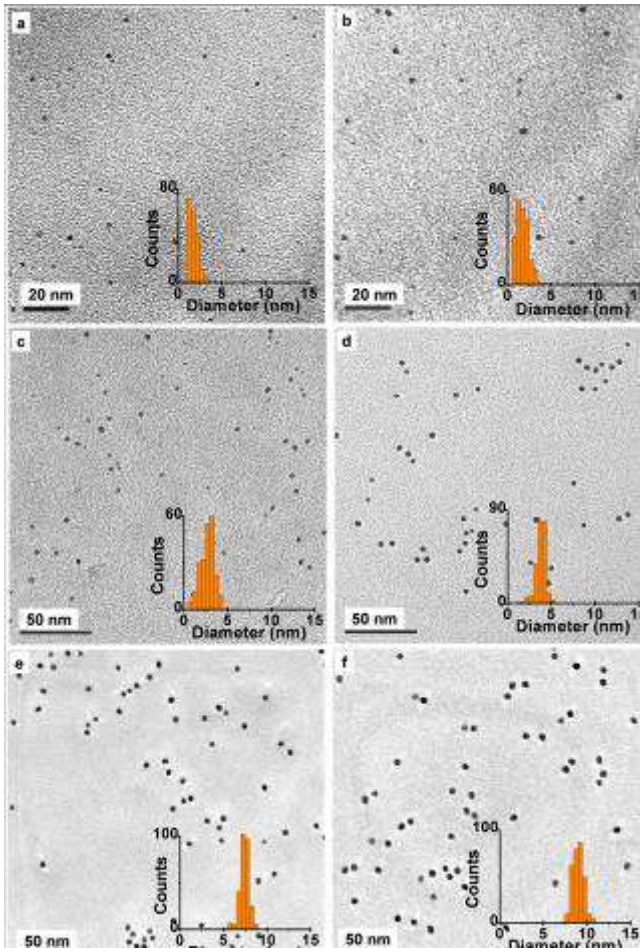

Figure 6. Representative TEM image of size-controlled nanoparticles formed by slow (dropwise) addition protocol. Insets show size distribution histograms. Nanoparticles were synthesized by slow (~ 1mL/min) addition of (a) 0.2 mL, (b) 0.4 mL, (c) 2 mL, (d) 5 mL, (e) 40 mL, of 0.64 mM chloroauric acid into 15 ml of 0.89 mM tannic acid., while maintaining reaction mixture pH above 6.4. The nanoparticle size distributions (μ ± σ) are (a) 1.7 ± 0.5 nm, (b) 1.8 ± 0.7, (c) 2.7 ± 0.8 nm, (d) 3.8 ± 0.6 nm, (e) 7.4 ± 0.6 nm. In (f) nanoparticles were synthesized by slow (dropwise) addition of 10 mL of 0.32 mM chloroauric acid solution into 15 mL of diluted gold colloid formed in experiment 'I'. Nanoparticle diameter (μ ± σ) = 9.1 ± 0.7 nm.

A simple mass balance for seeded growth shows that increase in mean nanoparticle diameter must be proportional to 1/3rd power of the moles (equivalent to volume at constant temperature) of chloroauric acid added. Figure 7 shows a plot of the predicted and the observed mean diameters as a function of the $1/3^{rd}$ power of the volume of chloroauric acid added. The observed values (including a few replicate samples) are seen to agree very well with the predicted values, which is a clear indication that the slow (dropwise) addition protocol is akin to one-shot process for seed formation followed by their controlled growth into nanoparticles.

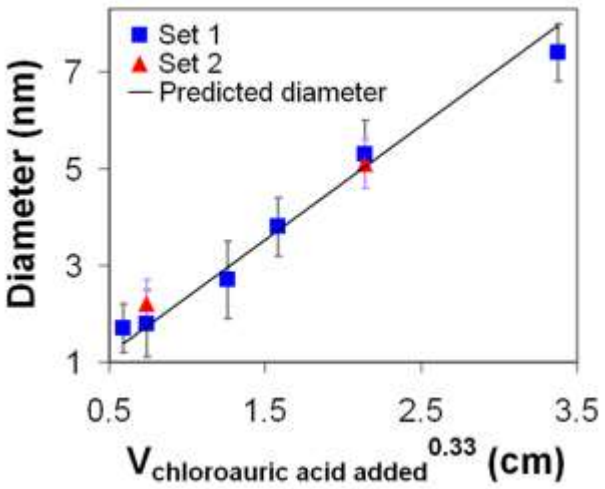

Figure 7. A plot of expected and observed nanoparticle diameter as a function of the amount of the 1/3rd power of the moles (equivalent to volume) of chloroauric acid added. The agreement between the predicted and observed diameters indicates that the slow (dropwise) addition process is akin to a one-shot nucleation-seeded growth process.

9.1.4. Summary

In summary, the present work reports a significant advance in terms of the realization of a simple, green process capable of synthesizing size-controlled gold nanoparticles rapidly under ambient conditions. The pH of precursor solutions, mode of contacting, and the dynamics of stabilizer adsorption vis-à-vis Brownian collision frequency are shown to be critical for tuning nanoparticle formation, growth, and coalescence. Thus, slower addition of chloroauric acid solution into tannic acid resulted in reduced polydispersity as compared to faster addition protocols. We have utilized such a slow (dropwise) addition protocol to synthesize size-controlled gold nanoparticles in the range of 2-10 nm within minutes at room temperature. The optimal process is shown to be similar to a one-shot nucleation-seeded growth technique and the growth mechanism is identified to be surface-reaction controlled under these conditions. These insights on independently manipulating reactivity and stabilisation can be extended to other redox reactions for rapidly synthesising size-controlled metal nanoparticles, as most systems exhibit pH dependent reactivity and stabilisation.

9.2 Plasma Processing of Nanoparticle Array for Enhanced Thermal Stability:-

Thermal stability of MPN arrays at high temperature is limited due to coalescence of nanoparticles induced by ligand desorption. Hence, it is essential to remove ligands from nanoparticle array. The ligand removal involves breakage of bonds and hence requires energy to be supplied. Jaeger et al. irradiated dodecanethiol capped array with electrons. They reported that the treated region remained stable to submersion in an organic solvent, while untreated area was washed away by the solvent. Spatz et al. formed gold nanoparticle arrays with interspacing ranging from 40-200 nm using diblock copolymers as templates and removed the polymer coating from the nanoparticles by using oxygen plasma treatment. Strehblow et al. demonstrated removal of alkanethiols from planar gold surfaces using plasma. It seems plausible that the thiol capping of the nanoparticles can also be removed without disturbing nanoparticle ordering by plasma treatment. Plasma treatment is also a technologically appealing parallel processing route, as compared to serial methods like e-beam treatment.
Plasma, a distinct state of matter, is basically an ionized gas comprised of ions, radicals, electrons and other neutral species. RF plasma is a gaseous discharge induced by radio frequency waves. A carrier gas is introduced into a chamber maintained at low pressure, and RF power is coupled to it. This results in dissociation of gas into chemically active species. These species bombard the specimen placed in the chamber and depending on the process conditions cause physical damage (sputtering) or chemically react with the substrate molecules. The unique property of plasma processing is that it occurs at relatively low temperatures (30-60º C). This property makes it ideal for the purpose of removing ligands from MPN arrays. However, over exposure of the array to the plasma also causes bombardment on nanoparticles and results in coalescence of nanoparticles. Hence, an optimised condition for removing the thiols without disturbing the ordering of the nanoparticle array should be identified.

9.2.1. Experimental methods and characterization techniques

Alkanethiol or polystyrene coated nanoparticles were synthesized using a phase transfer protocol from aqueous colloidal samples (nominally 5 nm gold nanoparticles) and MPN arrays were fabricated using method developed by Santhanam et al.

The arrays fabricated on a water surface were transferred to TEM grid or PDMS stamp through Langmuir Schaefer technique. Microcontact printing of nanoparticle array was used to transfer array to a desired substrate. Gatan plasma etching instrument (Solarus Model 950) and Milman reactive ion etcher (Milman RIE-1A) was used for plasma treatment of arrays. In Milman equipment, a turbo pump was used to achieve 10^{-5} mbar base pressure to remove contaminants. The electrodes and processing chamber were maintained at room temperature using cooling water. Dodecanethiol (DDT) capped nanoparticle array or thiol terminated polystyrene (PSSH) capped nanoparticle array were exposed to plasma. FEI tecnai F30 Transmission Electron Microscope (TEM) at 200KV was used for obtaining images. Zeiss ultra 55 Field Emission Scanning Electron Microscope (FESEM) was used for imaging. Image J software was used to analyze the images. Perkin Elmer Fourier Transform Infra Red (FTIR) spectrometer was used to obtain IR spectrum of the array stamped on quartz. The contact angle of water (3μm) on the array was measured using a Rame-harte Goniometer. Six reading of contact angle at different regions on the sample were measured and averaged. Atomic Force Microscopy (AFM), MFP-3D from Asylum research, was used to analyze the topography and cross section of the array. Contact mode AFM was used to clear a small patch (5 μm x 5 μm) on the printed array by using a high contact force (~ 150 nN) to act as a local reference for the base plane. A larger area which includes the cleared patch was then imaged in Tapping mode. This procedure was used to determine height of the array before and after plasma treatment. For thermal stability analysis, the nanoparticle arrays on the substrate was heated in a muffle furnace at required temperature.

9.2.3. Results and discussion

9.2.3.1. Effect of processing gas

The optimum plasma conditions required to remove ligands, without disturbing the order of the array, was found for '5 nm' dodecanethiol coated array. The arrays were exposed to Radio Frequency (RF) plasma for different duration. The gas used was a mixture of O_2 and H_2 with flow rates of 6.4 sccm and 27.5 sccm respectively. Figure 8 shows nanoparticle array exposed to plasma for different duration. Higher duration of exposure of nanoparticle array to plasma resulted in highly interconnected nanostructure. The optimum condition for the 5 nm nanoparticle array is exposure at 20 W power and 10 s time period.

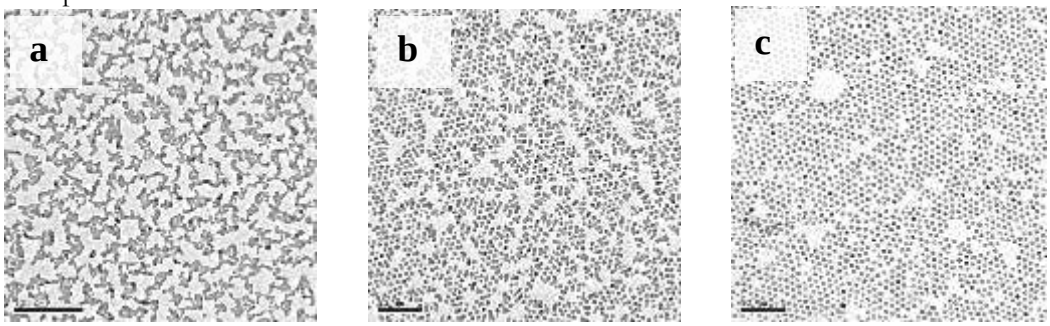

Figure 8: TEM image of array with nanoparticle array exposed to different plasma conditions. (a) Power = 50 W, Duration = 30 s, Scale bar = 100 nm (b) Power = 20 W, Duration = 20 s, Scale bar = 100 nm (c) Power = 20 W, Duration = 10 s, Scale bar = 100 nm.

Raiber et al. studied the removal of alkanethiol SAMs on planar gold surfaces using RF plasma. They reported that hydrogen plasma requires more time to remove the layer of alkanethiolin comparison to an oxygen plasma. In the plasma treatment discussed above, a mixture of hydrogen and oxygen was used to generate plasma. The treatment time for the optimum condition was 10-20 s and exposure time is quite short. If the plasma is generated using only hydrogen gas, then the time for treatment will increase and will offer more control over the removal of thiol. Experiments were carried with plasma generated with hydrogen gas at flow rate of 20 sccm. An array made of nanoparticles of nominal diameter 7 nm was exposed to plasma for different time periods. When array was exposed for 60 s, nanoparticles coagulated and at 50 s there was loss of ordering. The order of the nanoparticle array remained undisturbed at 45 s and was identified as optimum condition to treat such arrays. Figure 9 shows TEM images of the array after processing for different durations in a hydrogen plasma environment.

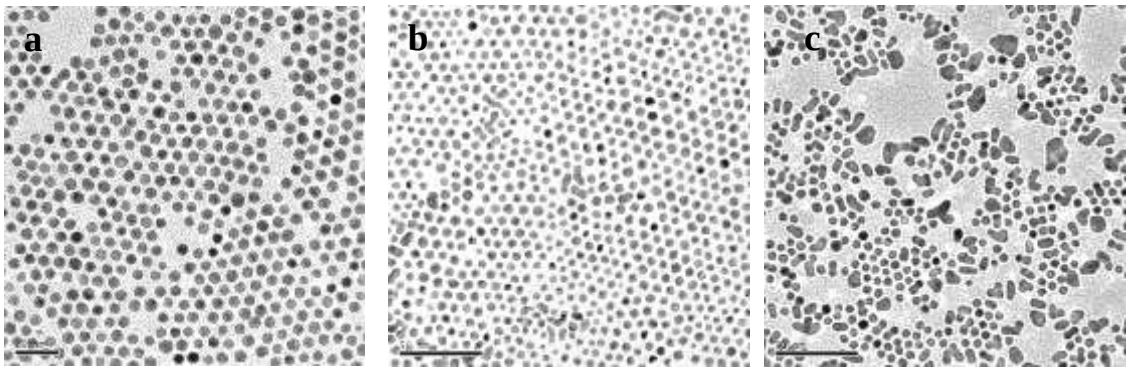

Figure 9: RF power = 20 W, Hydrogen gas only. (a) TEM image of array treated for 45 s. Scale = 20 nm. (b) TEM image of array treated for 50 s. Scale = 50 nm. (c) TEM image of array treated for 60 s. Scale = 50 nm.

Exploratory experiments performed in Gatan plasma cleaner showed the existence of optimal range of exposure beyond which nanoparticle array coagulates. Gatan plasma cleaner has poor control over operating pressure and temperature. Further experiments were carried out in Milman reactive ion etching system which has more controlled environment. The turbo pump was used to achieve very low base pressure. The water cooled chamber and electrode ensures that the substrate does not heat up during plasma treatment.

9.2.3.2. Optimization of plasma conditions

The time duration of plasma treatment is the key parameter to control the removal of ligands from nanoparticle array. A higher window of time duration of plasma treatment is desirable to achieve more reproducible protocol. Hence, the impact of parameters other than time duration like operating pressure and RF power were investigated.
At operational pressure of 0.15 torr, the effect of RF power on hydrogen plasma treatment of DDT capped nanoparticle was explored. In a given time duration of plasma treatment (45 s), higher RF power (30 W) results in coagulation of nanoparticles in array than at lower RF power (20 W). Figures 10a and 10b show FESEM image of nanoparticle treated at RF power 30 W and 20 W. Higher RF power results in higher ionic density in plasma and hence nanoparticles coagulate. Hence it is essential to have low RF power. In case of operational pressure, for a given timescale of plasma treatment, higher operational pressure (1.5 torr) results in coagulation of nanoparticles. Figure 3c and 3d shows FESEM image of nanoparticle treated at plasma pressure of 0.15 torr and 1.5 torr. Higher RF power and higher pressure results in higher ionic density in plasma and hence nanoparticles coagulate. Hence it is essential to have low RF power and low pressure.

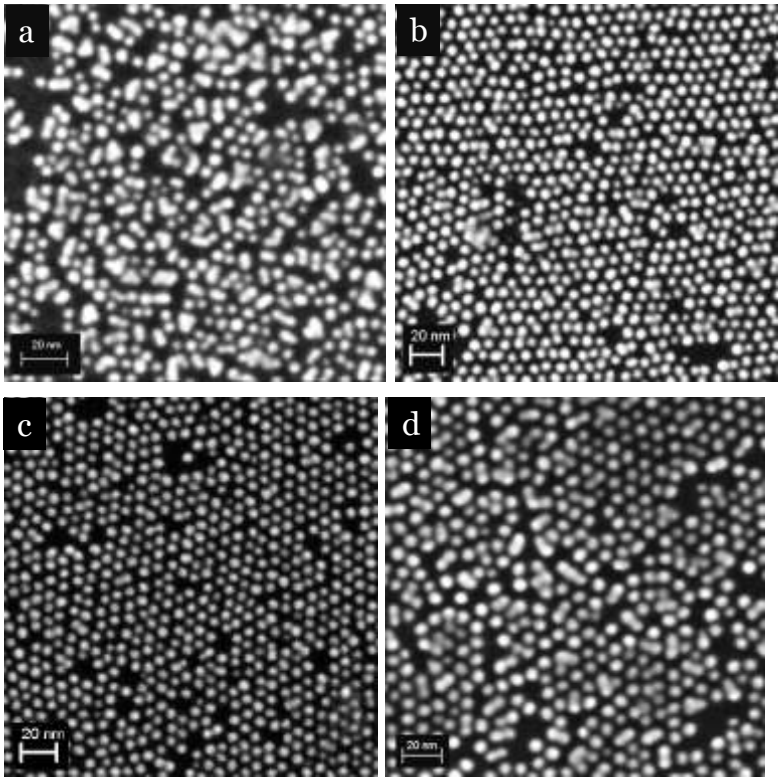

Figure 10: Pressure = 0.15 torr. Time duration = 45 s (a) FESEM image of array treated at RF power 30 W. Scale = 20 nm. (b) FESEM image of array treated at RF power 20W. Scale = 20 nm. (c) FESEM image of array treated at pressure 0.15 torr. RF power = 20 W. Scale = 20 nm. (d) FESEM image of array treated at pressure 1.5 torr. RF power = 20 W. Scale = 20 nm.

A minimum RF power is required to initialize plasma. The minimum RF power required for plasma at different operating pressures were investigated. Figure 11 shows RF power required to initialize plasma as a function of pressure. Initially, as pressure decreases the RF power required to initialize plasma decreases. But below an optimal pressure, 0.6 mbar, power required to initialize plasma increases. Hence further experiments were carried at the optimum pressure.

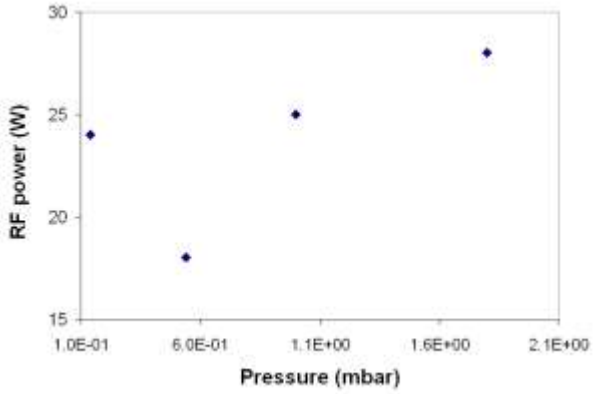

Figure 11: Minimun RF power required to initialize plasma at different pressure

9.2.3.3. Plasma treatment of DDT capped and PSSH capped nanoparticle array

DDT capped gold nanoparticle array was exposed to hydrogen plasma at optimized pressure and RF power. Figure 12 shows FESEM images of nanoparticle array exposed at different time duration. The time exposure of 45 s was identified as optimum. Thiol terminated polystyrene capped nanoparticle array, with interparticle spacing 13 nm, was exposed to hydrogen plasma to remove polystyrene. On hydrogen plasma treatment, nanoparticle array coalesced to form globules of polystyrene-gold nanoparticle structures. FESEM image, figure 12c and 12d, shows that size of nanoparticle in the agglomerate structure remains same. Polystyrene has unsaturated carbon bonds and exposure to hydrogen plasma may result in cross linking of these bonds. Hence, oxygen plasma treatment was investigated. Operational pressure and RF power was optimized as carried out for hydrogen plasma. Oxygen plasma treatment of 7 minutes was observed to be the optimum for

20,000 MW polystyrene capped nanoparticles, while 12,000 MW polystyrene capped nanoparticle array required 4 minutes of plasma treatment. Figure 5e and 5d shows image of polystyrene capped nanoparticles after exposure to oxygen plasma.

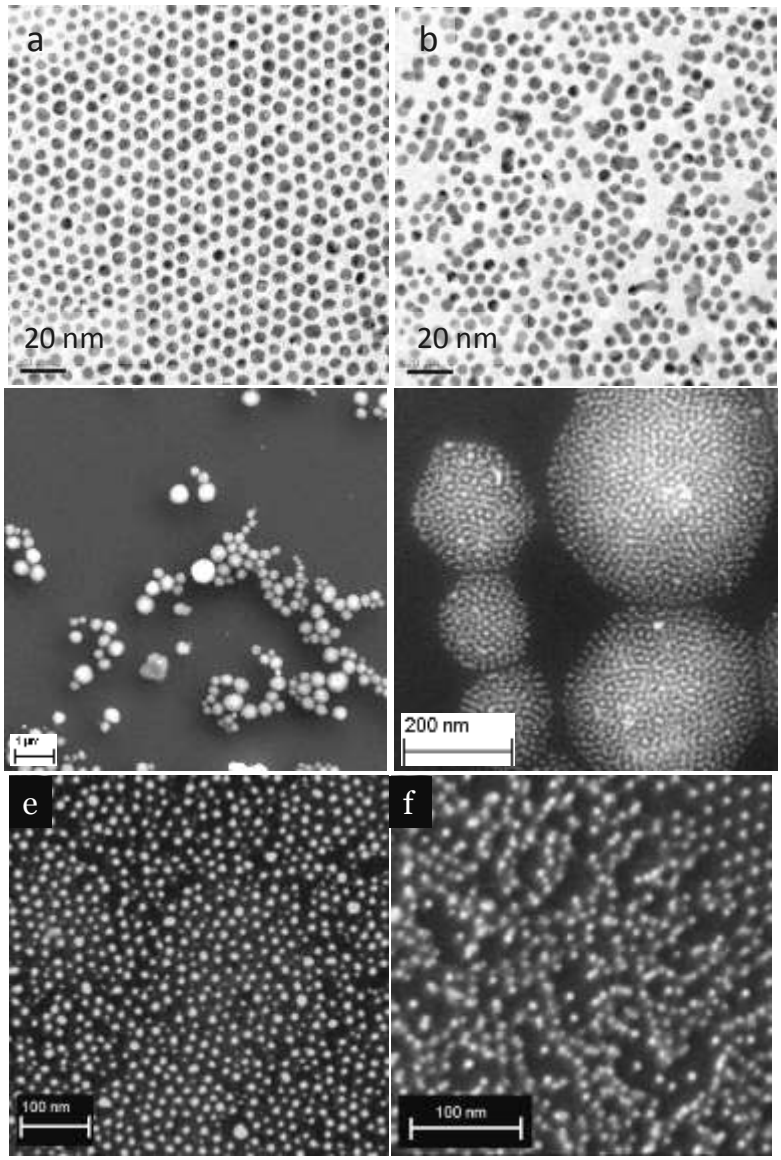

Figure 12: (a) TEM image of array treated for 45 s. Scale = 20 nm. (b) TEM image of array treated for 60s. Scale = 20 nm. (c) FESEM image of hydrogen plasma treated array. Scale = 1 μm. (d) High magnification image of hydrogen plama treated array. Scale = 200 nm. (e) FESEM image of PSSH capped nanoparticle array after 9 minutes of oxygen plasma treatment. Scale = 100 nm. (f) FESEM image of PSSH capped nanoparticle array after 11 minutes of oxygen plasma treatment. Scale = 100 nm.

9.2.3.4. Microcontact printing of plasma treated nanoparticle array

During plasma treatment of nanoparticle array, the substrate too is exposed to plasma. If plasma interaction with substrate results in undesired change in properties, plasma treatment of array on substrate may not be suitable. For example, oxygen plasma treatment of silicon wafer causes charge traps in surface and changes its electrical properties. Hence, it is essential to develop a method to transfer plasma treated nanoparticle array. Nanoparticle array on PDMS was treated with hydrogen plasma. But the microcontact printing of such plasma treated arrays was not possible because of the increased adhesion between surface and nanoparticles. Hence, polyethylacrylate (PEA), an organic soluble polymer/elastomer, was used to pick nanoparticle array from Teflon cell. After exposing to plasma, adhesion between nanoparticles and polyethylacrylate increases. Hence, microconatct printing will not result in transfer of nanoparticles. Polyethylacyrlate stamp with nanoparticle array was placed over a silicon wafer and left in toluene at 60 °C. After 24 hours, polyethylacrylate dissolves and leaves behind the nanoparticle array. The nanoparticle array was subjected to further characterization to analyze the effect of plasma treatment. Scheme 1 shows the different methods of plasma treatment and transfer of nanoparticles.

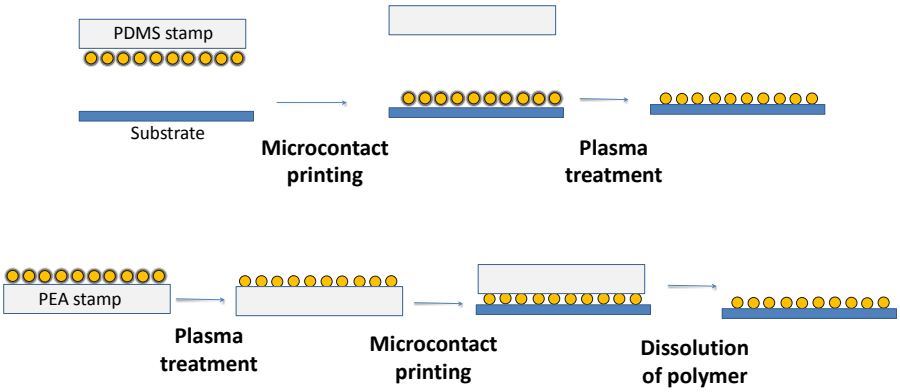

Scheme 1: Microcontact printing using PDMS/PEA stamp and plasma treatment

9.2.3.5. Atomic force microscopy characterization of nanoparticle array

The cross sectional height of DDT capped nanoparticle array, before and after plasma treatment, was analyzed through atomic force microscopy. DDT capped nanoparticle array (average TEM diameter – 7nm) on a silicon substrate was studied using AFM. Three square patches of length 5 μm were made using contact mode AFM. These patches were used as lithographic markers to image the same place. The average cross sectional height of the array obtained from all three windows was 9 - 9.5 nm. The length of a dodecanthiol molecule is 1.6 nm. This shows that the net increase in height, with respect of size of nanoparticles, is 2 – 2.5 nm. The array was subjected to hydrogen plasma and imaged again. Figure 13a shows the cross sectional height of array before and after plasma treatment. The cross sectional height of the array is reduced on average by ~1.5 – 2 nm in all three windows. The reduction in the height is attributed to the removal of thiol molecule from the nanoparticles.
Similarly, the cross sectional height of polystyrene (20000 MW) capped nanoparticle array was analysed during different time periods of oxygen plasma treatment. Figure 13b shows the cross sectional height at different plasma exposure. The overall height of the array is 42 nm while the diameter of nanoparticle is 7 nm. The cross sectional height decreases linearly with time and after 10 minutes of plasma exposure, cross sectional height reaches 7 nm which is equivalent to diameter of nanoparticle. The reduction in cross sectional height indicates the removal of polystyrene ligand from the nanoparticle.

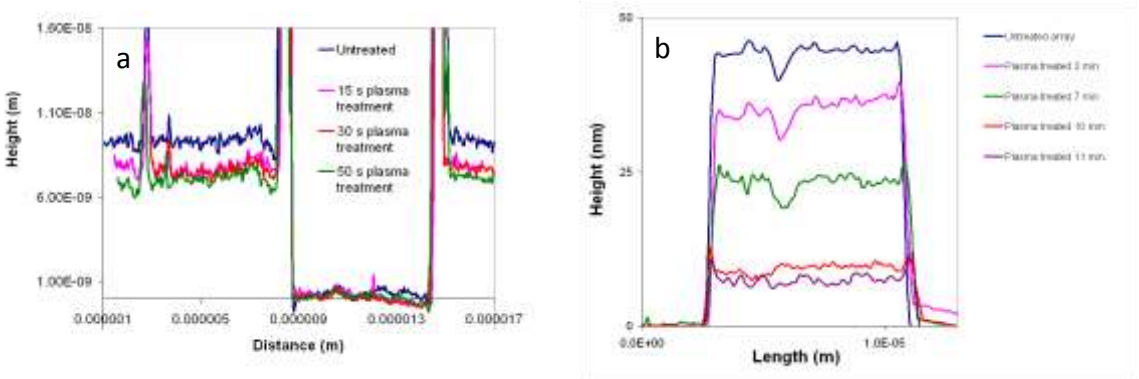

Figure 13: (a) Cross sectional height of DDT capped nanoparticle array before and after plasma treatment (b) Cross sectional height of thiol terminated polystyrene capped nanoparticle array before and after plasma treatment

9.2.3.6. FTIR characterization of nanoparticle array

The arrays stamped onto quartz substrates were treated at the optimized condition. The FTIR spectra of the array were taken before and after treatment. A special holder was designed to hold the quartz plate at fixed position. The FTIR spectrum shows the presence of methylene stretching bonds at 2920 cm^{-1}. Figure 14a shows FTIR spectra of DDT capped nanoparticle array before and after treatment. The decrease in the signal indicates the removal of dodecanethiol ligand. The nanoparticle array treated on polyethylacrylate and transferred to substrate too shows decrease in the signal corresponding to dodecanethiol. In the case of polystyrene capped nanoparticle array, the signal in FTIR corresponding to polystyrene decreases significantly. Figure 14b shows FTIR spectra of thiol terminated polystyrene capped nanoparticle array before and after oxygen plasma treatment.

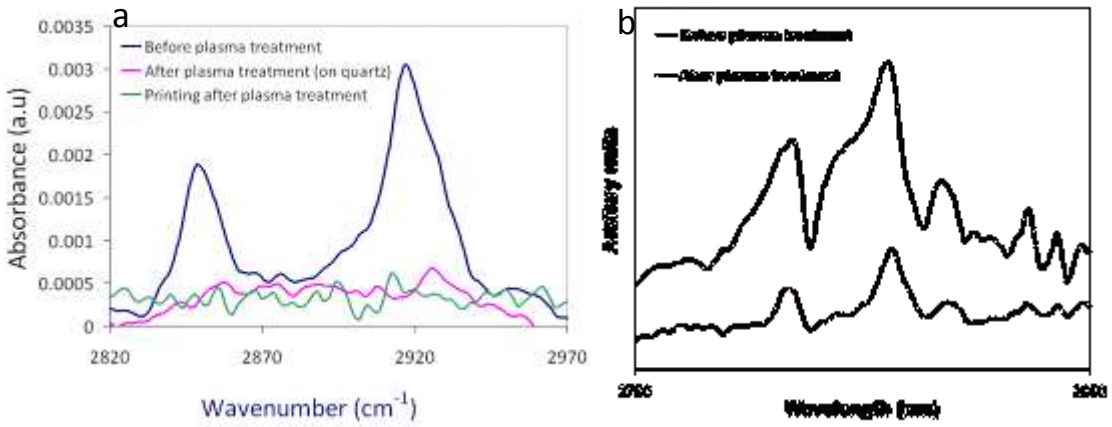

Figure 14: (a) FTIR spectra of DDT capped nanoparticle array before and after treatment showing methylene strech bands (b) FTIR spectra of thiol terminated polystyrene capped nanoparticle array before and after plasma treatment

The contact angle of a water droplet (3 μl) on DDT capped nanoparticle array was measured before and after exposure to hydrogen plasma. The contact angle of water on plain quartz is 33^{o} and on DDT SAM is 115^{o}. After plasma treatment, the contact angle on the nanoparticle array decreases to 47 ± 2^{o} from 93 ± 3°C (before treatment), indicating the decrease in the hydrophobicity of the surface. This can only be due to decrease in area of exposed hydrocarbon chains and an increase of exposed gold/quartz surfaces (having lower contact angle).

9.3. Thermal Stability of Nanoparticle Array

Nanostructured materials have gained interest among researchers due to their unique size dependent properties. Nanomaterials have potential applications in many fields like electronics[1], photonics[1], biochemical engineering, catalysis etc. Use of nanostructured materials in devices can reduce the cost and increase the efficiency of device. To realize nanomaterial based applications, it is essential to possess a simple method to fabricate nanostructures. Self-assembly of nanoparticles into an ordered array, a bottom-up approach is one such simple technique for fabrication. Self-assembled ordered array has applications in many fields like magnetic storage device, non-volatile memory device, as ordered templates for nanowire growth etc. One of the challenges in application of nanoparticle array is the thermal stability of array. Some of the applications of nanoparticle array require stability at high processing temperatures. Thermal stability of nanoparticle array has been investigated to understand the limits of applications. Hardy et al. showed that electrical property of dodecanethiol capped nanoparticle array changes dramatically at higher temperatures and on cooling the original properties are not retained. Hardy et al. studied the optical properties of nanoparticle array at higher temperatures and showed that on heating the optical property changes permanently. Fabrication of magnetic FePt nanoparticle array requires annealing at high temperatures and particles coagulate at these temperatures. Nonvolatile memory application requires deposition of insulators and contacts at high temperatures. Nanowire growth utilizing VLS growth requires ordered nanoparticle array stable at high temperatures (650 °C). Addressing the thermal stability of nanoparticle array will result in realizing the commercial applications of nanoparticle array at large scales.

9.3.1. Results and discussion

Gold nanoparticle array with nominal diameter of 7 nm were fabricated on large scale. The interparticle spacing between the nanoparticles was 2 nm for the dodecanethiol (DDT) capped nanoparticles and 13 nm for thiol terminated polystyrene (PSSH) capped nanoparticles. In case of thiol terminated polystyrene, the interspacing can be simply varied by varying the molecular weight of polystyrene.
Figure 15a, 15b and 15c shows the TEM images of DDT capped nanoparticle array treated at 25°C, 200°C and 500°C for 1 hour on silicon nitride substrate. The mean size of nanoparticles is 33.1 nm and 59.0 nm respectively. Thermal stability of DDT capped nanoparticle array on silicon wafer substrate showed a different behavior. The mean size of nanoparticles treated at 200°C and 500°C are 17.6 nm and 26.2 nm. The nanoparticle size is lesser than that obtained from silicon nitride substrate. Figure 15d shows the diameter of gold nanoparticles at different temperature and on different substrate.

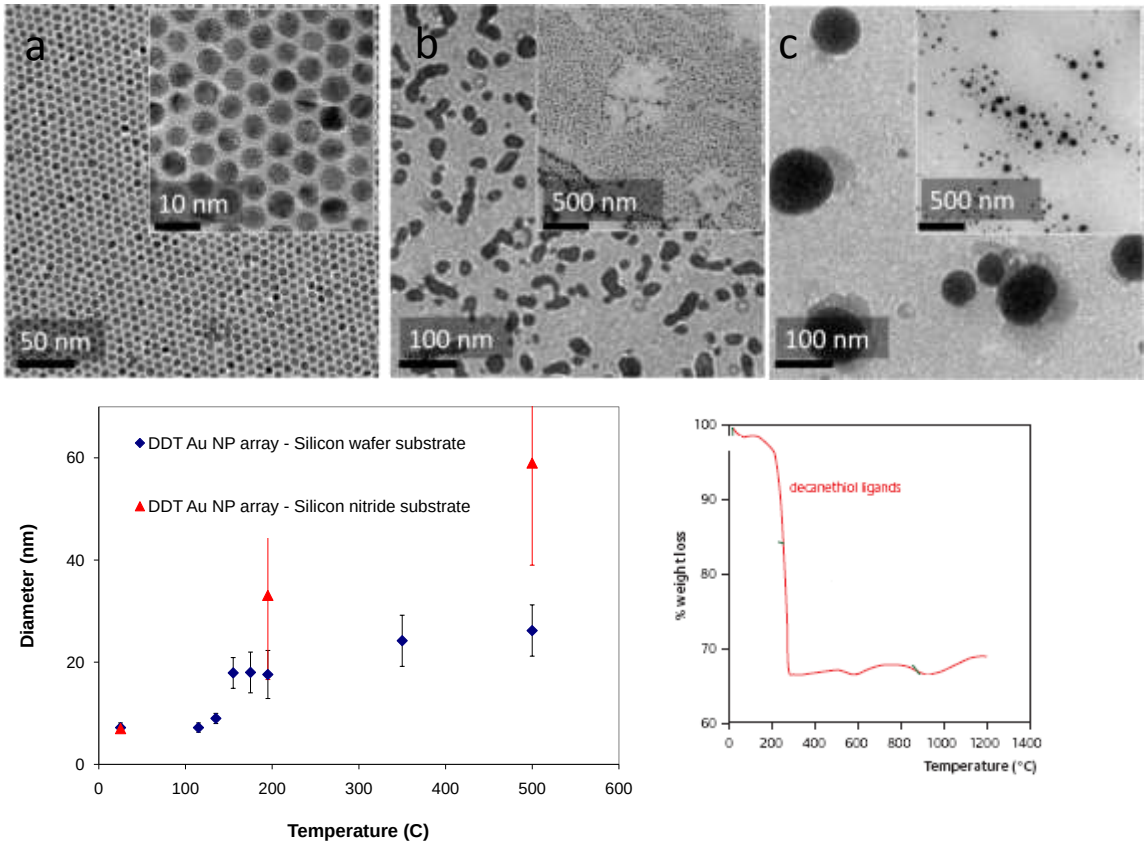

Figure 15: (a) DDT capped gold nanoparticle array at 25°C (b) DDT capped gold nanoparticle array at 200°C (c) DDT capped gold nanoparticle array at 500°C (d) Diameter of gold nanoparticles at different temperatures (e) Thermo gravimetric analysis of decanethiol capped nanoparticles from Hardy et al. for comparison.

Desorption of self-assembled monolayers of alkanethiol from gold substrate at higher temperatures is well documented phenomena. Figure 15e shows the thermo gravimetric analysis of decanethiol capped gold nanoparticles. The weight loss begins at 150 °C and rapid decrease is observed at 225 °C signifying the desorption process of DDT. However, during heat treatment, nanoparticles coagulate at 135 °C even before the complete desorption of DDT. The alkanethiol layers at higher temperature can become liquid-like and allow free movement of gold nanoparticles on the surface. Hence, the particles coagulate at 135 °C itself. At higher temperatures, above 350 °C, other phenomena like Ostwald ripening and surface diffusion of gold atoms are known to take place and hence the particle size increases. At high temperature, nanoparticles coagulate more in silicon nitride than silicon because of lower Hamaker constant of silicon nitride. The liquid like behaviour of ligands at high temperature causes mobility. With higher Hamaker constant, silicon restricts the mobility and hence coagulation is less on silicon.

Atomic force microscopy characterization of nanoparticle array was performed at different temperatures. Figure 16a shows topography of nanoparticle array at different temperatures. At 200 °C, the roughness of the nanoparticle array increases to 3 nm from 1 nm at 25 °C. The increase in roughness is due to the coagulation of nanoparticle. Figure 2b shows the cross sectional height of nanoparticle array at different temperatures. The cross sectional height of nanoparticle array decreases from 11 nm to 8 nm and the decrease in height corresponds to that of alkanethiol ligand. Eventhough the average diameter of nanoparticle increases to 17.6 nm at 200 °C, the cross sectional height is 8 nm.

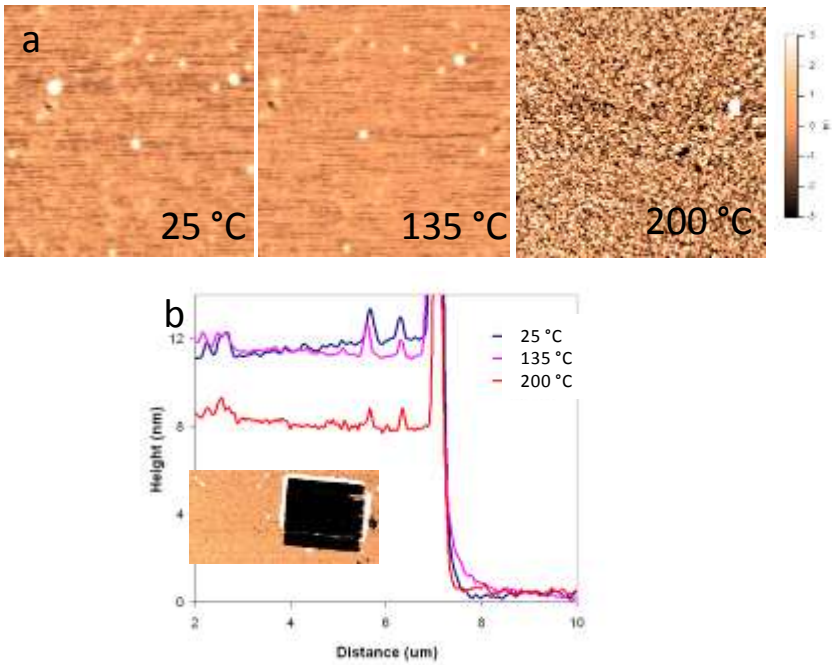

Figure 16: (a) AFM topography of nanoparticle array at 25 °C, 135 °C (b) and 200 °C (c). (d) Cross sectional height of array at different temperatures.

Thiol terminated polystyrene capped nanoparticle array are stable till 200 °C. At 250 °C, nanoparticles coagulate and further heating results in increase in mean diameter of nanoparticle. Figure 17a-17c shows thiol terminated polystyrene capped nanoparticle array at different temperatures. Thermogravimetric analysis of nanoparticles shows that desorption of polystyrene takes place after 275 °C. Figure 17f shows TGA of thiol terminated polystyrene capped nanoparticle array. Hence, polystyrene capped nanoparticle array shows better thermal stability at 200 °C than DDT capped nanoparticle array. Atomic force microscopic characterization of nanoparticle array shows that the desorption of polystyrene from nanoparticle at 275 °C is not uniform. Figure 17d and 17e shows the AFM image and cross sectional height.

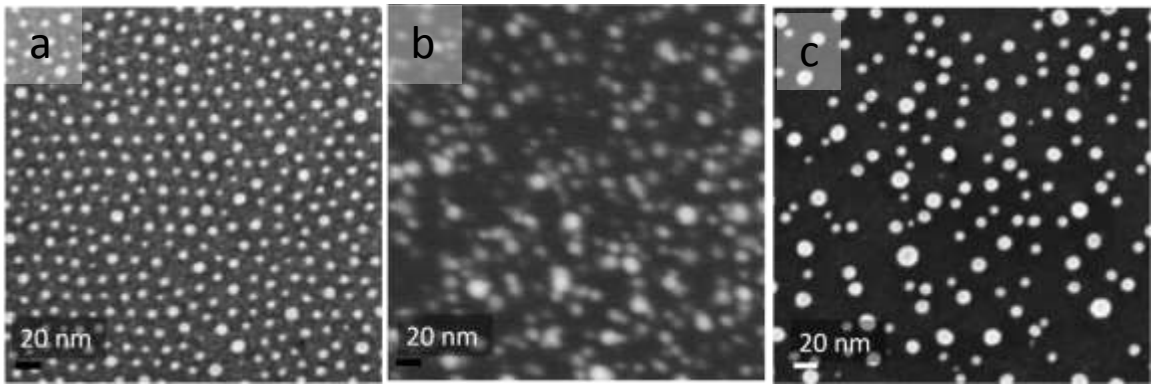

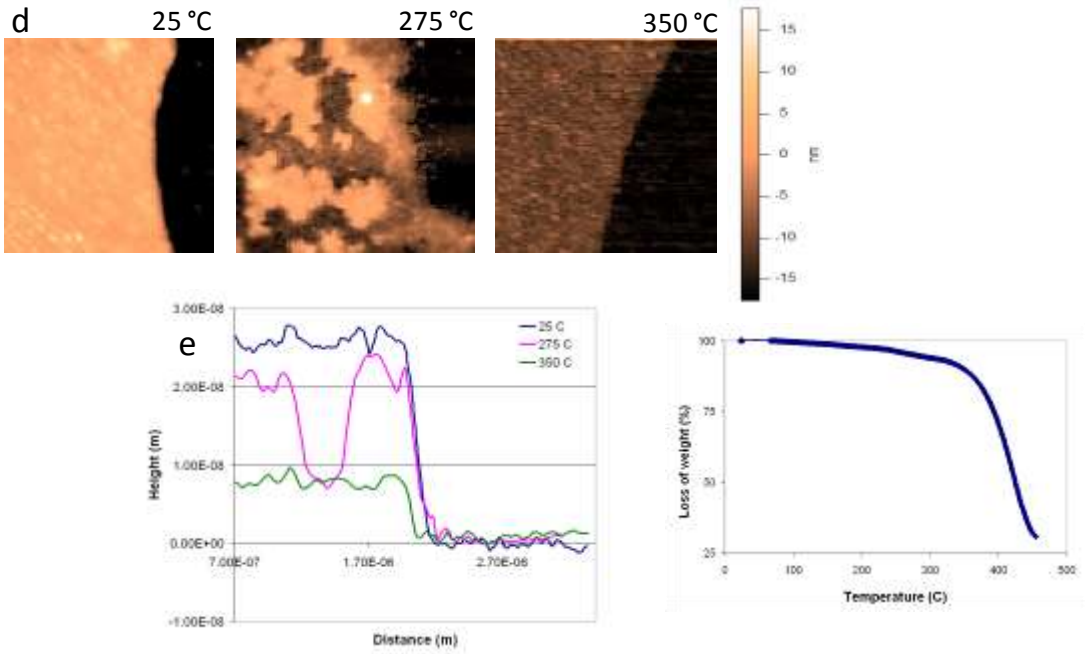

Figure 17: Thiol terminated polystyrene capped nanoparticle array at 200 °C (a), 275 °C (b), and 350 °C (c). (d) AFM topography of nanoparticle array at different temperatures. (e) Cross sectional height of nanoparticle array at different temperatures. (f) Thermo gravimetric analysis of PSSH capped nanoparticle array

Investigation of thermal stability of array shows that the onset of coagulation of nanoparticle array correlates with desorption of ligands. At high temperatures, ligands reach a liquid like behavior and the mobility of nanoparticles increases resulting in coagulation of nanoparticles. Hence, removal of ligands prior to heat treatment can make nanoparticles stable at higher temperature.

9.3.2. Thermal stability of plasma treated nanoparticle array

Plasma treated bare nanoparticle array with different interparticle spacing, 2 nm and 13 nm, were subjected to heat treatment. After plasma treatment, nanoparticle array with 2 nm interparticle spacing were stable at 200 °C, while untreated array coagulated at 150 °C. Figure 18a and 18b shows TEM image plasma treated nanoparticle array after heat treatment at 200 °C and 500 °C. Coagulation of nanoparticles during ligand desorption at high temperatures, 150-200 °C, has been prevented. But at higher temperatures, above 350 °C, mean diameter of nanoparticles increases due to other process like Ostwald ripening and surface diffusion. Figure 18a and 18b shows the comparison of mean diameter of nanoparticle array on silicon nitride and silicon wafer substrate after heat treatment at different temperatures.

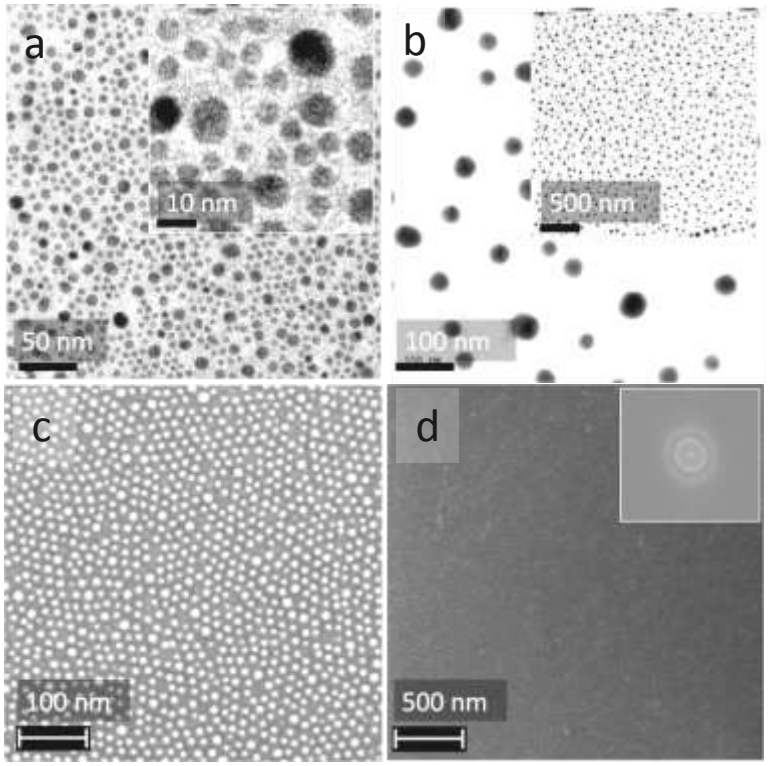

Figure 18: (a) TEM image of plasma treated DDT capped nanoparticle array at 200 °C and 500 °C (b). (c) FESEM image of thiol terminated polystyrene capped nanoparticles. (d) Long range ordered array of PSSH capped nanoparticle. Inset shows rings in Fourier transform of image indicating long range ordering.

Nanoparticle array with 13 nm interparticle spacing, after plasma treatment, remains stable even at 650 °C. Figure 18c and 18d shows plasma treated thiol terminated polystyrene array after heat treatment at 650 °C. Figure 19c shows the comparison of mean size of nanoparticles in plasma treated and untreated array on silicon wafer. By removal of ligands through plasma treatment, coagulation of nanoparticles at 275 -300 °C due to ligand desorption has been avoided

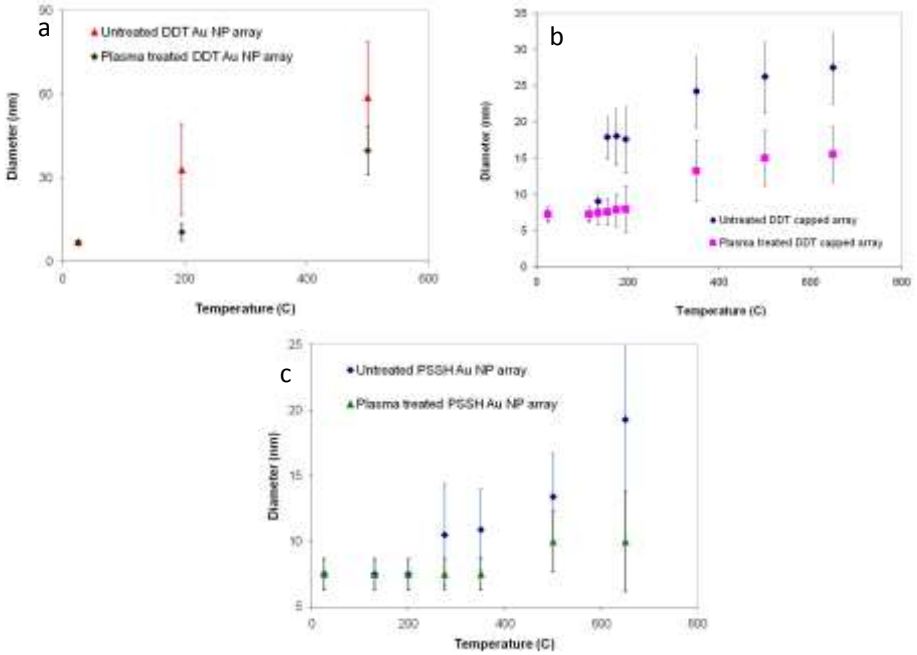

Figure 19: (a) Comparison of nanoparticle diameter in plasma treated and untreated DDT capped nanoparticle array on silicon nitiride and on silicon wafer (b). (c) Comparison of nanoparticle diameter in plasma treated and untreated thiol terminated polystyrene capped nanoparticles

10. Conclusions summarising the achievements and indication of scope for future work:

Summary of achievements:

The objectives of the proposal (given above) have been met and groundwork in terms of process development for solar energy conversion has been undertaken. Characterization of RF plasma processing by TEM, SEM, DLS, AFM, FTIR and contact angle measurements have been carried out, and have helped in elucidating the salient features of the process. A green protocol for the rapid, room-temperature synthesis of metal nanoparticles has been developed. The main conclusions are:

- Size-controlled, monodisperse gold nanoparticles in the range of 1-10 nm were synthesized within 10minutes at room temperature using a green reducing agent.
- RF plasma has been used to selectively remove the ligands (FTIR, AFM characterizations) in an MPN array without disturbing the lateral ordering, and both chemical stability and thermal stability is seen to be greatly enhanced post processing, and is only limited by interparticle spacing and nanoparticle melting point.
- Under optimal processing conditions, AFM characterization indicates that the ligand layers are removed as if a uniform reaction front (AFM cross-section profiling) is progressing downwards. There are two probable mechanisms for explaining such a result: a) the thiol ligands are mobile and diffuse on the surface at a rapid rate to maintain a homogeneous coverage on the particle, b) the particles are rotating to expose all sides evenly. The actual mechanism can only be probed using sophisticated x-ray characterization tools.
- Overexposure of closely packed nanoparticle arrays clearly show signs of aggregation at length scales corresponding to 3-4 nanoparticle diameters. However, based on projected area (TEM characterization)and AFM height analysis, there is no indication of three-dimensional agglomeration in these plasma irradiated films.
- By varying the ligand size, the interparticle spacing has been varied from 2 -15 nm and the core diameter was varied independently from 5-10 nm. It was found that larger interparticle spacing leads to greater thermal stability.

Innovations:

A simple and robust, room-temperature, aqueous phase protocol for size and shape-controlled nanoparticle synthesis has been developed. This is currently being used to characterize various reactor designs for continuous-flow synthesis of monodisperse nanoparticles.

RF plasma based processing of MPN arrays to form chemically and thermally stable bare metal nanoparticle arrays with interspacings of the order of particle diameters.

Scope for future work:

The batch protocol shows great promise for the development of a green, economically-viable continuous flow process for large scale synthesis of size-controlled metal nanoparticles. Such size-controlled gold nanoparticles are useful for bioconjugation of proteins in rapid assay tests based on Localised Surface Plasmon Resonance (LSPR). Forming ordered templates for growth of nanowire arrays by VLS process for further application in nanostructured solar cell architectures, and fabrication of nanoporous, conducting, electro-catalytically active membranes for fuel cell applications are being actively pursued in our group. Apart from these, bare metal nanoparticle arrays are also being characterized as the active layers in floating gate based memory devices.

11. S&T benefits accrued:

i. List of Research publications

S No	Authors	Title of paper	Name of the Journal	Volume	Pages	Year
1	S.K. Sivaraman, I.Elango, Sanjeev Kumar, V. Santhanam	A green protocol for room temperature synthesis of silver nanoparticles in seconds	Current Science	97(7)	1055-1059	2009

ii. Manpower trained on the project

a) *Research Scientists or Research Associates:* *None*

b) No. of Ph.D. produced: One in progress {Mr. Sankar Kalidas (Jan 2007 - date)}

c) Other Technical Personnel trained: Five

a. Mr. Alok Srivastava (M.E. Student, June 2006- June2007)
b. Ms. Shruti Seshadri (Project Asst. July 2006- May2007)
c. Ms. Prathima Yadav (Project Asst. July 2007- Sep2007)
d. Ms. Jency Daniel (Project Asst. Nov 2007- Jan 2008)
e. Mr. Vijay Jain(Project Asst. Apr 2008 – Nov.2009)

iii. Patents taken, if any

- ✓ S. Sankar Kalidas, V. Santhanam, "A method for preparing metal or metal oxide nanoparticles", IPO Chennai -- 775/CHE/2009 (patent pending), US application being filed.

12. Financial Position:

No	Financial Position/ Budget Head	Funds Sanctioned	Expenditure	% of Total cost
I	*Salaries/ Manpower costs*	3,60,000.00	3,76,205.00	7.58
II	*Equipment*	38,00,000.00	38,00,000.00	76.63
III	*Supplies & Materials*	1,50,000.00	1,49,993.00	3.02
IV	*Contingencies*	1,00,000.00	99,998.00	2.02
V	*Travel*	90,000.00	32,766.00	0.67
VI	*Overhead Expenses*	5,00,000.00	5,00,000.00	10.08
	Total			***100%***

13. Procurement/ Usage of Equipment
a)

S No	Name of Equipment	Make/Model	Cost (FE/ Rs)	Date of Installation	Utilisation Rate (%)	Remarks regarding maintenance/ breakdown
1	Reactive Ion Etcher	Milman/ RIE-1A [s]	38,00,000.00	10-07-2008	60%	Although, the equipment is currently working well, installation was delayed by one year because of supplier. Presently, Milman thin film systems is acting unprofessionally and is unwilling to support the instrument or respond to queries. If possible, MTFS Pvt.Ltd and its proprietors Dr.Milind Acharya, and Mandar Ashtikar could be blacklisted as vendors for future GOI projects!

b) Plans for utilising the equipment facilities in future

This equipment is now a workhorse for fabricating thermally, mechanically and chemically stable ordered nanoparticle arrays, whose applications in the following areas are currently being pursued; namely,

- fuel cell catalyst layers,
- synthesising nanowire arrays as photoanodes for Dye Sensitised Solar Cells,
- floating gate memory devices,
- patterned magnetic bit storage elements.

Name and Signature with Date

06-02-2010

*a.*_____

(S. Venugopal, Principal Investigator)

06-02-2010

*b.*_____

(Sanjeev Kumar, Co-Investigator)